Atmospheric Environment 264 (2021) 118715

Contents lists available at ScienceDirect

Atmospheric Environment

journal homepage: www.elsevier.com/locate/atmosenv

Nonlinear response of nitrate to NO_x reduction in China during the COVID-19 pandemic

Chuanhua Ren [a,b], Xin Huang [a,b,c,*], Zilin Wang [a,b], Peng Sun [a,b], Xuguang Chi [a,b], Yue Ma [a,b], Derong Zhou [a,b], Jiantao Huang [a,b], Yuning Xie [a,b], Jian Gao [d], Aijun Ding [a,b]

[a] Joint International Research Laboratory of Atmospheric and Earth System Sciences, School of Atmospheric Sciences, Nanjing University, Nanjing, 210023, China
[b] Jiangsu Provincial Collaborative Innovation Center of Climate Change, Nanjing, 210023, China
[c] Frontiers Science Center for Critical Earth Material Cycling, Nanjing University, Nanjing, 210023, China
[d] Chinese Research Academy of Environmental Sciences, Beijing, 100012, China

HIGHLIGHTS

- Enhanced secondary nitrate of aerosol particles were observed during COVID-19 lockdown.
- The emission reduction of NOx leaded to higher atmospheric oxidizing capacity and ammonia concentration.
- Elevated atmospheric oxidizing capacity and NH_3 further promotes nitrate formation.

GRAPHICAL ABSTRACT

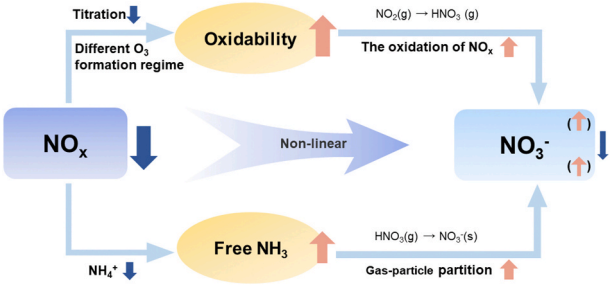

ARTICLE INFO

Keywords:
COVID-19
Emission reduction
Nitrate pollution
Enhanced NH_3
Ozone

ABSTRACT

In recent years, nitrate plays an increasingly important role in haze pollution and strict emission control seems ineffective in reducing nitrate pollution in China. In this study, observations of gaseous and particulate pollutants during the COVID-19 lockdown, as well as numerical modelling were integrated to explore the underlying causes of the nonlinear response of nitrate mitigation to nitric oxides (NO_x) reduction. We found that, due to less NO_x titration effect and the transition of ozone (O_3) formation regime caused by NO_x emissions reduction, a significant increase of O_3 (by ~ 69%) was observed during the lockdown period, leading to higher atmospheric oxidizing capacity and facilitating the conversion from NO_x to oxidation products like nitric acid (HNO_3). It is proven by the fact that 26–61% reduction of NO_x emissions only lowered surface HNO_3 by 2–3% in Hebi and Nanjing, eastern China. In addition, ammonia concentration in Hebi and Nanjing increased by 10% and 40% during the lockdown, respectively. Model results suggested that the increasing ammonia can promote the gas-particle partition and thus enhance the nitrate formation by up to 20%. The enhanced atmospheric oxidizing capacity together with increasing ammonia availability jointly promotes the nitrate formation, thereby partly offsetting the drop of NO_x. This work sheds more lights on the side effects of a sharp NO_x reduction and highlights the importance of a coordinated control strategy.

* Corresponding author. School of Atmospheric Sciences, Nanjing University, Nanjing, 210023, China.
E-mail address: xinhuang@nju.edu.cn (X. Huang).

https://doi.org/10.1016/j.atmosenv.2021.118715
Received 19 May 2021; Received in revised form 21 August 2021; Accepted 2 September 2021
Available online 8 September 2021

1. Introduction

Atmospheric aerosol, especially fine particles ($PM_{2.5}$), has drawn increasing attention due to its negative impacts on both air quality and human health (Brook et al., 2010; Kim et al., 2015). As the world's second-largest economy, China has experienced severe air pollution caused by increasing coal consumption, motor vehicle usage and industrial production, which are linked to the rapid economic development (Xu et al., 2013). In 2013, the annual mean $PM_{2.5}$ concentration reached up to 75 μg m^{-3}, and the daily concentration even exceeded 500 μg m^{-3} during the winter hazy days. Such extreme and aggravating haze pollution has triggered extensive public alarm and aroused the attention of scientific research. Many studies proposed that secondary inorganic compositions like sulfate, nitrate, and ammonium (SNA) played a dominant role (>50%) in the severe haze in China (Wang et al., 2020; Chan and Yao, 2008; Yang et al., 2011).

To mitigate air pollution, the State Council of China promulgated the toughest-ever Air Pollution Prevention and Control Action Plan in 2013 (China State Council, 2013). This air pollution control chiefly focused on the reduction in primary emissions of sulfur dioxide (SO_2) and nitrogen dioxide (NO_2), which are the main precursors of SNA. As expected, the Action Plan has achieved drastic emission reduction. From 2013 to 2017, the average national emissions of SO_2, NO_x, and primary $PM_{2.5}$ decreased by 59%, 21%, and 33%, respectively (Ding et al., 2019; Wang et al., 2019; Zhang et al., 2019). Despite the remarkable air quality improvements, air pollution in China remains severe (Zhang et al., 2019). For instance, 70.7% of cities in China failed to meet the national standard of annual $PM_{2.5}$ (35 μg m^{-3}) in 2017. And serious pollution events, particularly secondary pollution, still frequently happen. The severe particulate pollution (daily mean $PM_{2.5}$ concentrations larger than 150 μg m^{-3}) days observed in Beijing-Tianjin-Hebei (BTH) and Yangtze River Delta (YRD) was 31 and 25 days in 2017 winter, separately (Li et al., 2019). Meanwhile, many observations revealed that the contributions of nitrate to $PM_{2.5}$ have continuously increased and have become the main cause of severe pollution in China since 2013 (Xu et al., 2019a; Wen et al., 2018). For example, in Beijing 2018), secondary nitrate was the largest source, accounting for 25.7% of the annual measured $PM_{2.5}$, and during the heavily polluted days, the contribution from nitrate even reached 57.5% (Huang et al., 2021). Similarly, in Nanjing, nitrate had the highest annual average concentration (12.8 ± 11.4 μg m^{-3}) among all bulk species during 2017–2018 (Yu et al., 2020). In Chengdu, long-term observations from 2015 to 2017 indicated that the concentrations of sulfate and ammonium have been well reduced, but nitrate did not show a similar decrease (Kong et al., 2020).

Since the end of January 2020, the Coronavirus Disease 2019 (COVID-19) first outbroke in China. Due to the rapid growth of the confirmed case number and deaths, the Chinese government has implemented various policies against the COVID-19 pandemic, including traffic restrictions and stay-at-home orders involving more than 1.3 billion people (Xinhua News, 2020). With the lockdown policy strictly enforced, transportation and industrial production were dramatically decreased, and thereby posing a direct impact on air pollutant emissions. For instance, it was found that daily concentrations of SO_2, NO_2, and CO during the lockdown period were reduced by 31.3%, 60.4%, and 3% respectively, compared to the same period in 2019 (Filonchyk and Peterson, 2020). However, the air quality in eastern and northern China did not improve prominently as expected, for instance, several cases of heavy haze pollution occurred in BTH, YRD, and Hubei province (Chang et al., 2020; Li et al., 1994; Shen et al., 2021). Despite a large reduction (~60%) in NO_x emissions, nitrate is still the dominant component of $PM_{2.5}$ in Nanjing and Beijing. Both the nitrate pollution during COVID-19 and the increased nitrate proportion from 2013 to 2017 signify that it is crucial to identify the key factors of nitrate formation to alleviate the increasing trend of nitrate pollution.

The outbreak of COVID-19 provides an exceptionally unique opportunity to assess the relationship between air pollution and anthropogenic emissions, particularly the responses of nitrate chemistry to NO_x emission reduction. Based on the special experiment introduced by COVID-19 lockdown, this study aims to shed more lights on the less nitrate improvement than expected in eastern China. Here, we first compared the concentration of pollutants during the pre-COVID and lockdown period with the in-situ observational data. And then a chemical box model was used to unravel the relationship between nitrate and its precursors. Besides, we performed parallel experiment simulations by a chemical transport model with different emission scenarios to examine the impact of COVID-19 emission reductions on nitrate and HNO_3. In general, by integrating both observations and simulations, this work aims to explore the nonlinear response of nitrate to its precursors, which unearths an explanation for still serious nitrate pollution despite substantial reductions of NO_x. The conclusions of the study can help us examine the effectiveness of air emission reduction policies, which may help mitigation of nitrate pollution in the future.

2. Data and methods

2.1. Observational stations and instrumentation

To better understand the regional-scale air pollution, observation dataset of four sites (Fig. 1) in Beijing-Tianjin-Hebei (BTH), Yangtze River Delta (YRD), and Central China (CC) were used to analyze the air pollutants concentrations in pre-COVID (1–24 January 2020) and the COVID-lock periods (26 January −17 February 2020).

For the BTH region, one of the field observations is conducted at the Chinese Research Academy of Environmental Sciences (CRAES) (40.05° N, 116.42° E) in Beijing. The sample inlet is approximately 4 m above the ground and 46 m above sea level. This site is surrounded by university buildings, 300 m northeast of a densely trafficked major road (Gao et al., 2016). Another site of the BTH region is conducted in Hebi City Ecological Environment Bureau (35.73° N, 114.30° E). The site is surrounded by government buildings, schools and residential areas. Both two sampling sites in BTH could be representative of an urban district with the mixed influence of residual, traffic, and construction emissions. For the YRD region, the site is located in the Station for Observing Regional Processes of the Earth System (SORPES) in Nanjing, which is a regional background station in the western part of the YRD region (32.11° N, 118.95° E) (Ding et al., 2013, 2019). The station is located on the top of a 40 m hill, inside Nanjing University Xianlin Campus, 20 km northeast of downtown Nanjing (Shen et al., 2018). For the CC region, the $PM_{2.5}$ composition data was obtained from the Changsha Malingpo air quality monitoring station (28.20° N, 113.08° E).

In all these four sites, online sampling instruments are set to measure key meteorological parameters, the concentrations of gaseous pollutants and the water-soluble inorganic ion component of $PM_{2.5}$ concentration. A commercially available Monitor for Aerosols and Gases in ambient Air (MARGA, MetrohmLtd., Switzerland) was used to measure the hourly $PM_{2.5}$ concentration water-soluble ions (NH_4^+, SO_4^{2-}, NO_3^-, Na^+, K^+, Ca^{2+}, Mg^{2+}, Cl^-) and inorganic gases (NH_3, HNO_3, HCl) (Sun et al., 2018; Xie et al., 2015). The MARGA instrument was calibrated on an hourly basis using internal standard liquid (LiBr) to ensure a stable and reliable ion chromatograph. And the organic carbon (OC), and elemental carbon (EC), were measured by a field semi-online OC/EC analyzer from Sunset Laboratory Inc. (USA) with a $PM_{2.5}$ cyclone inlet applied to measure OC/EC in aerosol. To avoid bias in measuring OC, volatile organic compounds were removed by a carbon parallel-plate diffusion denuder (from Sunset Lab) equipped to the device (Gao et al., 2016). Additionally, the hourly $PM_{2.5}$, SO_2, NO_2, O_3, and CO data were obtained from China's air quality monitoring networks, which can be archived at the air monitoring data center of the Ministry of Ecology and Environment of China. The meteorological data, including wind direction, wind speed, temperature, precipitation and relative humidity were directly obtained from NCDC Integrated Surface Database (ISD).

2.2. Regional chemical transport model

To quantitatively understand the response of air quality in the pre-COVID and COVID-lockdown period, regional coupled dynamical and chemical simulations were conducted based on WRF-Chem model (Weather Research and Forecasting model coupled with Chemistry, version 3.7.1). WRF-Chem is an online three-dimensional, Eulerian model that includes physical and chemical processes such as emission and deposition of pollutants, advection and diffusion, gaseous and aqueous chemical transformation, aerosol chemistry and dynamics, etc (Grell et al., 2005). The model has been widely used and evaluated against measurements, which has been further improved by optimizing the parametrization of aqueous and heterogeneous chemistry in Asia (Huang et al., 2014). In this study, the model domain was centered at 35° N and 110° E with a 20 km × 20 km spatial resolution to cover eastern China and its surrounding areas. On vertical distribution, 30 vertical layers were set from the surface to the top pressure of 50 hPa, and 10 of them were set below 1 km to better resolve the processes within boundary layer (Wang et al., 2018).

The simulation was conducted from December 1, 2019 to February 14, 2020. The initial and boundary meteorological conditions were set by 6-hourly 1° × 1° National Center for Environment Prediction (NCEP) global Final (FNL) reanalysis data. Surface and global upper air observational weather data of wind, temperature and moisture from NCEP Automated Data Processing (ADP) were assimilated to improve the reproduction of meteorological fields. The physics and chemical processes schemes used in this study are summarized in Table 1.

Table 1
WRF-Chem model configuration options.

Physical and chemical processes	Scheme
Boundary layer	YSU
Land surface	Unified Noah
Microphysics	Lin (1983)
Cumulus parameterization	Grell-Devenyi
Longwave radiation	RRTMG
Shortwave radiation	RRTMG
Gas-phase chemistry mechanism	CBMZ
Aerosol scheme	MOSAIC

Natural emissions such as biogenic, sea salt (Gong et al., 1997) and dust (Shaw et al., 2008) were included online into the model runs for this study. Biogenic emissions were calculated online by MEGAN (Model of Emissions of Gases and Aerosols from Nature) module. It estimated the net emission rates of isoprene, monoterpene and other biogenic VOCs from terrestrial ecosystems into the above-canopy atmosphere. In addition to natural emissions, the anthropogenic emissions of CO, NO_x, SO_2, NH_3, BC, OC, $PM_{2.5}$. PM_{10} and VOCs were set based on the MEIC database (Multi-resolution Emission Inventory for China) (Li et al., 2017). To quantitatively understand the emission-triggered perturbations on air pollution, two parallel experiments with different emission scenarios were designed: (i) standard emission levels in 2017 (Run_std), (ii) the same as (i) but reducing the anthropogenic emissions with the up-to-date reduction ratio during the lockdown period (Run_reduction) (Huang et al., 2020; Zheng et al., 2021). And the simulation well

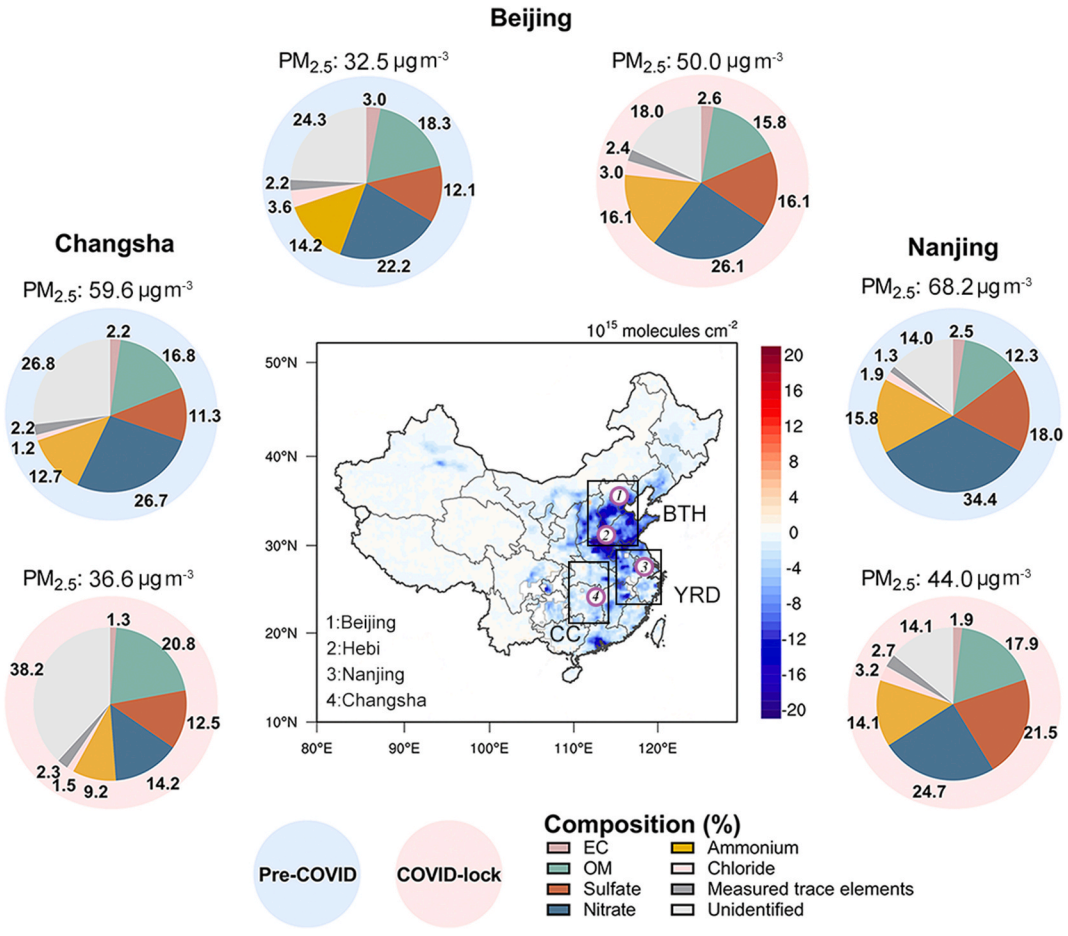

Fig. 1. Comparison of the median daily $PM_{2.5}$ concentrations (μg m^{-3}) and hourly average chemical components friction (%) in different observation sites. The pies with blue underpainting mean pre-COVID period, and the red underpainting represents COVID-lockdown period. The inner picture is a spatial distribution of NO_2 column concentration reduction due to the COVID-19 lockdown from OMI satellite. The black rectangles represent the three focused regions in eastern China. (For interpretation of the references to colour in this figure legend, the reader is referred to the Web version of this article.)

reproduced the observation of the $PM_{2.5}$ chemical components in three cities (Figs. S5–S7).

2.3. Chemical sensitivity box modelling

A zero-dimensional chemical box model was configured to simulate the non-linear relationship between nitrate and NO_x. It couples the lumped structure photochemical mechanism CBMZ (including 154 chemical reactions) to account for gas-phase atmospheric chemistry (Zaveri and Peters, 1999). To examine the relationships between nitrate formation and its precursors, we conducted a series of scenarios simulations with the initial concentrations of NO_x varying from 0 to 80 ppb (at intervals of 10 ppb) according to existing field measurements across China. Observed concentrations obtained from ground measurements during the COVID-19 period were used to drive the box model as initial conditions (listed in Table S1). However, the VOCs measurements were not made during the present study, so we used the average simulation data derived from WRF-Chem model output for approximation. As for meteorological conditions, the box model was initialized with lockdown period averaged meteorological measurements at 12:00 UTC taken in Beijing to represent the typical atmospheric stratification in wintertime. Each numerical experiment was conducted for a time period of 24 h.

2.4. ISORROPIA-II thermodynamic equilibrium model

The formation of nitrate depends on the reversible reaction of the chemical equilibrium between gas-phase HNO_3 and NH_3, and particle-phase NH_4NO_3. The gas-particle equilibrium is temperature-dependent (Seinfeld and Pandis, 2016). The ISORROPIA-II (available at http://isorropia.eas.gatech.edu/) is a thermodynamic equilibrium model that can be used to determine the phase state and composition of an NH_4^+-SO_4^{2-}-NO_3^--K^+-Ca^+-Mg^+-Na^+-Cl^--H_2O aerosol system with its corresponding gas components in thermodynamic equilibrium. To estimate the effects of temperature changes on NH_3 concentrations, we fixed measurements of water-soluble ions and used temperature and relative humidity (RH) during pre-COVID and COVID-lockdown periods as input data. In this study, ISORROPIA-II was run in the "forward mode", assuming particles were "stable" with solid precipitates in low RH.

2.5. Ambient free ammonia indicator

To quantity the availability of ambient free ammonia in two periods, the observed molar ratio (R) of total ammonia ($TA = NH_3 + NH_4^+$) to the sum of sulfate, total chlorine and total nitrogen ($TN = NO_3^- + HNO_3$) minus Na^+, K^+, Ca^{2+} and Mg^{2+} was chosen as an observable indicator (Xu et al., 2019b).

$$R = \frac{TA}{2SO_4^{2-} + NO_3^- + HNO_3(g) + Cl^- + HCl(g) - 2Ca^{2+} - Na^+ - K^+ - 2Mg^{2+}} \quad (1)$$

$R > 1$ means NH_3-rich environment where particulate NO_3^- formation is HNO_3 limited. $R < 1$ is the opposite and means NH_3 is limited.

3. Results and discussion

3.1. Observational evidence of enhanced secondary nitrate aerosol during lockdown

The air pollution measurements in pre-COVID and COVID-lockdown periods provided an insight into the air pollution with different emission levels. Based on $PM_{2.5}$ observations with good data coverage and quality control in three region sites, the comparison of $PM_{2.5}$ chemical compositions in different regions and the whole change of NO_2 column concentration are shown in Fig. 1.

As displayed in Fig. 1, despite the sudden reduction in primary emissions during COVID-19 lockdown, the daily $PM_{2.5}$ concentrations in Beijing, Nanjing, and Changsha are still worse than China's 35 μg m^{-3} standard and 4–5 times higher than the WHO's $PM_{2.5}$ guideline value of 10 μg m^{-3} (World Health Organization Occupational and Environmental Health Team, 2006). Unexpectedly, frequent $PM_{2.5}$ spikes were observed during COVID-lock period especially in Beijing and the overall $PM_{2.5}$ level in three cities was practically indistinguishable from that of the past three years for the same time in the calendar (Figs. S1 and S2). Although NO_x featured the largest decrease of all pollutants in Beijing and Nanjing, the mass fraction of nitrate can reach around 25% and it is still the dominant component in $PM_{2.5}$. Unlike two northern cities, the proportion of nitrate in Changsha has dropped significantly from 26.7% to 14.2%. Such a nonlinear relationship of nitrate and NO_x emissions degradation as well as regional differences inspires us to further investigate the underlying causes. Generally, particulate nitrate is formed by two major pathways. In the daytime, the NO_2 can be oxidized by OH radicals to form HNO_3, which is subsequently neutralized by NH_3 to produce ammonium nitrate (NH_4NO_3) (Calvert and Stockwell, 1983). In dark conditions, the reaction of NO_2 and O_3 produces the nitrate radical (NO_3·), which forms an equilibrium with N_2O_5 that can be subsequently taken up onto particles to enhance nitrate aerosol (Pathak et al., 2009, 2011; Brown and Stutz, 2012).

To analyze the impact of the precursor reduction on nitrate formation, the concentrations of these pollutants are compared in the pre-COVID and COVID-lock periods in Fig. 2. Consistent with satellite observations in Fig. 1, the near-surface NO_2 concentration also declined sharply (by ~ 61%) during the COVID-lockdown period in all three cities. However, the O_3 concentration increased significantly (by ~ 69%) due to the smaller titration of NO and the decrease of NO_x in a VOC-limited environment. Previous studies also indicate that the changes in the VOCs composition due to amount use of disinfectants containing compounds such as alcohols and carbonyls may also play a role in O_3 increase (Peralta et al., 2021). Besides, increased concentration of NH_3 was observed in Hebi and Nanjing, which might be contributed by rapid NO_x emission reduction and the volatilization of

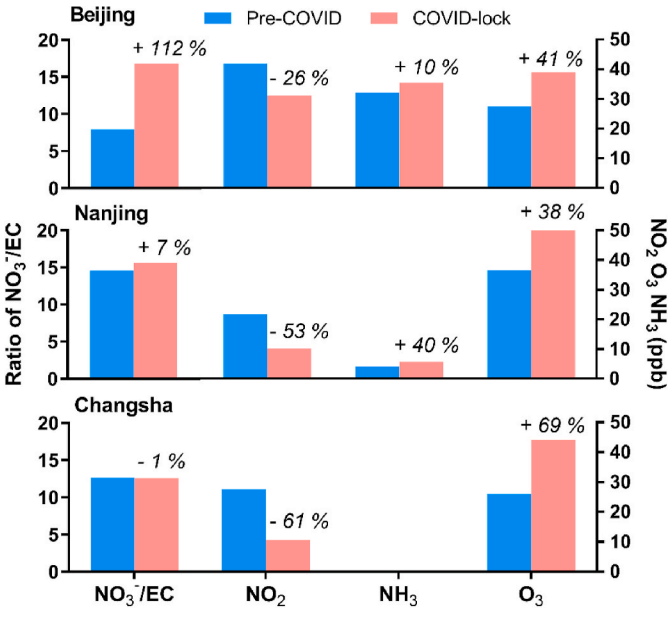

Fig. 2. Comparison of average NO_3^-/EC, NO_2, NH_3, O_3 concentrations and relative change (%) during the pre-COVID (blue bar) and COVID-lock (red bar) periods in Beijing, Nanjing and Changsha three ground sites. Due to the lack of NH_3 observation in Beijing, NH_3 data in the Beijing subgraph were provided by the Hebi site. Note: NO_2, NH_3 and O_3 are the averages of their daily maximal concentration for each period, and NO_3^-/EC is the hourly average concentration. (For interpretation of the references to colour in this figure legend, the reader is referred to the Web version of this article.)

NH_3 from the massive use of ammonia-based household cleaners during lockdown (discussed in Section 3.3). Compared with SNA, EC is mainly from primary emission, so the relative concentration of nitrate and EC can provide an insight into secondary nitrate formation (Huang et al., 2020). In spatial distribution, the nitrate production in northern China showed an increase in the lockdown period, especially in Beijing (+112%). On the contrary, there was no obvious change in Changsha (−1%). Such variations of nitrate production were consistent with the variations of nitrate friction in three cities displayed in Fig. 1, where Beijing showed the highest increasing level, followed by Nanjing and Changsha. The increment of nitrate friction (by ~ 4.1%) in Beijing was possibly due to the strengthened secondary nitrate production (by ~ 112%). Due to the negative effect caused by enhanced nitrate production, we further analyzed the secondary products in the process of nitrate formation.

Since that nitrate has different formation mechanisms during the day and night, we analyzed the diurnal cycle differences of NOR (nitrogen oxidation ratio, NOR = $[NO_3^-]$]/($[NO_3^-]$ + $[NO_2]$), O_3, NO_2, HNO_3, N_2O_5 and particulate nitrate between two periods. Fig. 3 shows the concentration changes ([lock]–[pre]) or relative changes ([lock]–[pre])/[pre]) of the abovementioned species at the same diurnal time. Owing to NO_x reduction during lockdown period, evident changes of the NO_2 diurnal cycle can be observed at all 3 cities, especially with much higher reduction at night time. Contrary to NO_2, the change of O_3 shows a significant opposite pattern, with evident increase at night, except for Changsha. Many studies have shown that NO_x reductions relax OH depletion by NO_x and in turn produce more O_3. Besides, NO_x reductions can increase O_3 concentration by reducing NO_x titration (via NO + O_3 as well as nocturnal NO_2 + O_3 reactions) (Leung et al., 2020). Due to these effects, a distinct increase was observed in O_3 in three sites. It is noteworthy that the patterns of diurnal differences between two periods in NOR, O_3 and HNO_3/N_2O_5 are similar. Owing to the rising oxidizing capacity caused by O_3, the production rate of HNO_3 and N_2O_5 was enhanced, pattern of which is consistent with the higher NOR displayed in Fig. 3. In Hebi and Nanjing, with the more efficient nitrogen oxidation at night, the HNO_3 showes an inapparent decrease though a sharp decline in NO_2.

Different from cities in northern China, the increase of O_3 peaks during the daytime (6:00–15:00) in Changsha. Due to the lack of observations on HNO_3 concentration, WRF-Chem simulated N_2O_5 data was analyzed showing in Fig. 3c. Since N_2O_5 is easily photodegraded during the day, the concentration of N_2O_5 does not change obviously in the daytime although O_3 levels increase significantly. At night, the slightly increase in O_3 concentration is not enough to offset the impact of NO_x decline, so the concentration of N_2O_5 drops a lot. The above observational analysis shows that the increase in O_3 can partly offset the reduction of NO_x and promote the production of HNO_3 and N_2O_5. At the same time, there are spatial differences between northern China and the CC region.

3.2. Facilitated atmospheric oxidation induced by NOx reduction

To shed more lights on the mechanism behind the observed phenomenon mentioned in Sect. 3.1, a series of scenario experiments based on the chemical box model were conducted. Ozone, an important oxidant for the formation of nitrate, is formed from emissions of NO_x and VOCs in the presence of sunlight. Therefore, O_3 formation is complicated by its association with the abundance of NO_x and VOCs. Fig. 4a shows the relationship between NO_x and O_3 concentrations. In the NO_x-limited regime, NO_x is short-supply, and O_3 is effectively formed with rising NO_x concentrations. However, as the concentration of NO_x increases, O_3 formation becomes VOCs-limited. Freshly emitted NO rapidly reacts with O_3, leading to NO_2 formation and O_3 depletion (titration process). Close to the sources, such titration process can be considered as a main O_3 sink. In addition, high NO_2 concentrations deflect the initial oxidation step of VOCs by forming other products (e.g., nitric acid and PAN), which prevents the net formation of O_3 (Xu et al., 2021). As presented in Fig. 4a, all of the three megacities with relatively high industry and traffic emissions are located at VOCs-limited regime, consistent with previous results (Yang et al., 2020). With the NOx reduction during COVID-lock period, the O_3 chemistry moves to NO_x-limited/mixed sensitive regime which leads to an increase in O_3, consistent with the phenomenon observed in the three cities.

In addition to O_3, OH radicals and NO_3 radicals are also important atmospheric oxidants in nitrate formation during day and night, respectively (Saiz-Lopez et al., 2017). In a VOCs-limited regime, the reduction of NO_x can release OH radicals that were originally depleted by NO_x, leading to an increase in OH, the same as ozone pattern. At night, NO_3 radical is generated by the reaction of NO_2 with O_3 and is dominantly depleted by freshly-emitted NO. Consequently, NO_3 radical

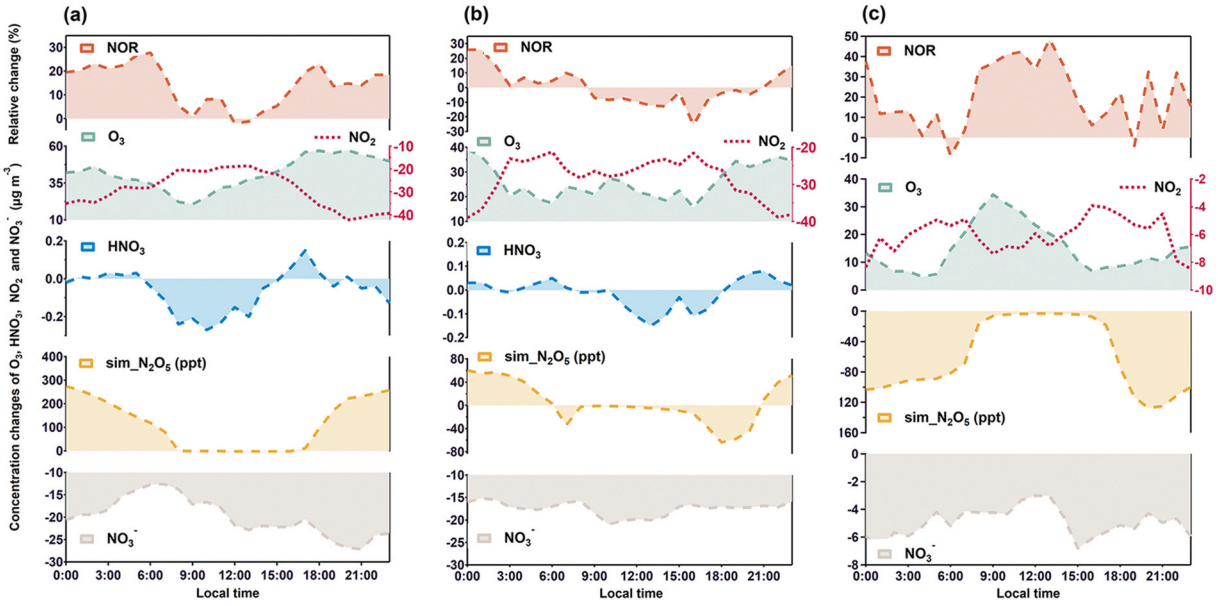

Fig. 3. Diurnal cycle of observed changes in NOR, O_3, HNO_3 and NO_3^- (unit: μg m^{-3}) between the COVID-lock and pre-COVID periods in **(a)** Hebi, **(b)** Nanjing and **(c)** Changsha station. Variations of N_2O_5 concentrations (unit: ppt) are provided with WRF-Chem simulations.

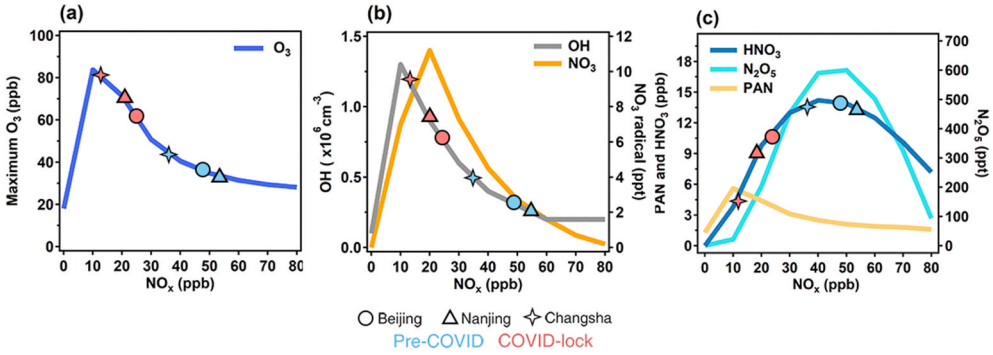

Fig. 4. **(a)** Box model simulated maximum O_3 concentration as a function of the initial concentrations of NO_x (0–80 ppb), **(b)** average OH radical (grey) and NO_3 radical (yellow) concentrations, **(c)** average HNO_3 (dark blue), N_2O_5 (light blue) and PAN (yellow) concentrations. Three shapes of symbols indicate the observed NO_x concentrations in three sites. The blue fill symbols mean pre-COVID period and red ones represent COVID-lock period. (For interpretation of the references to colour in this figure legend, the reader is referred to the Web version of this article.)

concentration soared by two times because of a simultaneous NO reduction and O_3 increase, as shown in Fig. 4b. As the oxidants increase, the production efficiency of HNO_3, N_2O_5 and PAN is enhanced even though their precursor NO_x dropped significantly. Under the joint influence of NO_x, OH and NO_3, the concentrations of HNO_3 and N_2O_5 reach their peak where NO_x is between 40 and 50 ppb. The NO_x levels in three cities during different periods are marked in Fig. 4. Although the increase in O_3 in the three cities is similar (Fig. 4a), their resultant HNO_3 concentration varies greatly due to their different initial NOx concentrations (Fig. 4c). The main source of NO_x resulting from human activities is the combustion of fossil fuels especially fuel used in cars. According to the MEIC inventory in 2017 (Li et al., 2017), the NO_x emission rate in Beijing, Nanjing and Changsha are 1.03, 1.32 and 0.63 Mg km^{-2} per month, respectively. For northern cities (Beijing and Nanjing), NO_x is about to reach the tipping point of HNO_3 during the pre-COVID period and HNO_3 concentrations still maintain relatively high after NO_x reduction. For Changsha, due to the less NO_x emission intensity, the initial concentration of NO_x is much lower than two other cities. Hence, the NO_x concentration during pre-COVID period has passed the tipping point, and HNO_3 and N_2O_5 drops sharply during the lockdown period in Changsha. PAN is an important indicator for photochemical pollution, forming similarly as O_3 in the photochemistry of certain VOCs and NO_x. The exclusive formation pathway of PAN is the termination reaction of peroxyacetyl radical ($CH_3C(O)O_2$, PA) with NO_2 (Liu et al., 2021). As PA comes mostly from the OH/NO_3/O_3 oxidation of a subset of oxygenated VOCs (OVOCs) in the box model, PAN and the above oxides have a similar relationship pattern which both reach the peak when NO_x is approximately 10 ppb.

In addition to the box model, we further conducted 3-dimensional regional simulation using WRF-Chem to explore the sensitivity to different NOx reduction rates (from 10% to 90%) in three regions. In Fig. 5, it clearly shows that the sharp reduction in NO_x emissions causes

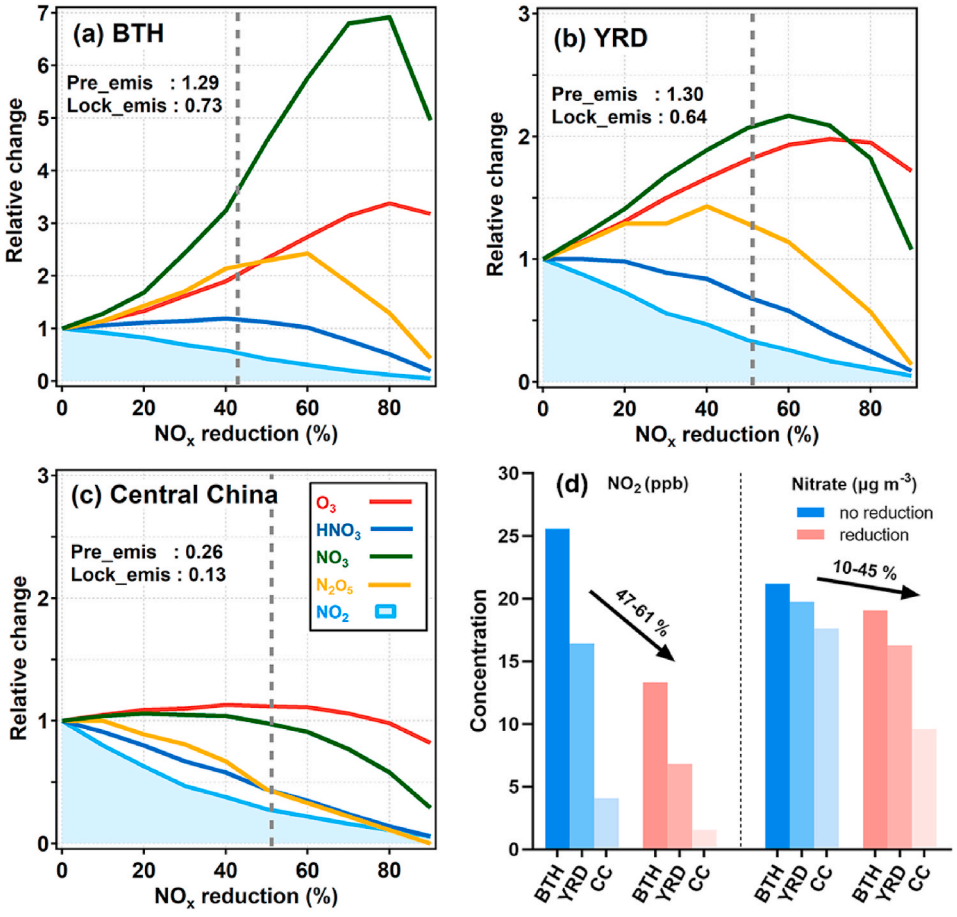

Fig. 5. Changes of O_3, HNO_3, NO_3 radical, N_2O_5 and NO_2 as a function of NOx emission reduction in the **(a)** BTH, **(b)** YRD and **(c)** Central China regions. The total NO_x emissions during Pre-COVID and COVID-Lock periods in three regions are shown in the upper left of each subgraph (unit: Mg km^{-2} per month). **(d)** NO_2 and nitrate concentration during the COVID-lockdown period for WRF-Chem runs with "reduction" (red) and "no reduction" (blue) emission scenarios, respectively. (For interpretation of the references to colour in this figure legend, the reader is referred to the Web version of this article.)

a substantial increase of O_3, NO_3 radicals and hence a nonlinear response of oxidation products like HNO_3, and N_2O_5 in all three regions. However, there exist great regional disparities. The oxidizing capacity increment in BTH is most evident, followed by YRD and the CC. This regional difference may be caused by two factors: meteorology and precursors concentration (precursor emissions levels). From the perspective of meteorology, O_3 formation highly depends on two meteorological factors including the ultraviolet (UV) radiation that drives photolysis to trigger the chain reaction, and temperature, which affects the reaction kinetics rates (Wang et al., 2017). In the CC, due to higher solar radiation intensity and temperature, the O_3 production is more efficient, and it can quickly make up for the O_3 deficiency caused by the titration effect, and thus presents a weaker response to precursor NO_x reduction compared with the other two northern regions. From the view of precursor emissions, according to the bottom-up inventory, the NO_x emission intensity in BTH, YRD and the CC are quite different during the pre-COVID, which are 1.29, 1.30, 0.26 Mg km^{-2} per month, respectively. Much lower base concentrations of NO_x caused by weaker emissions in the CC region makes the NO-titration less sensitive to the NO_x reduction, and thus the O_3 enhancement is not that obvious. The NO_x emission reduction and little response of O_3 led to the fact that HNO_3 and N_2O_5 decline much more substantially than other regions, as displayed in Fig. 4c. To quantify the impact of NO_x reduction on nitrate concentration, we performed another simulation by fixing meteorological conditions in the lockdown period while varying emissions for pre-lockdown (no reduction) and COVID-lockdown (reduction) periods to truncate meteorological effects. As displayed in Fig. 5d, the nitrate concentration in BTH, YRD, and CC three regions decreased by 10%, 17%, and 45%, respectively.

3.3. Elevated NH_3 further promotes nitrate formation

As an important alkaline gas in the atmosphere, NH_3 plays a crucial role in nitrate formation by neutralizing nitric acid to form nitrate ammonia. Fig. 2 shows that the average surface NH_3 during COVID-19 increased by 10%, and 40% compared to pre-COVID levels over Hebi and Nanjing, respectively. NH_3 concentrations can be affected by NH_3 emissions and the partitioning of NH_3 to NH_4^+. Generally, the rising ambient temperature will promote the transition of ammonia from NH_4^+ to gaseous state NH_3. As shown in Fig. S8, with the arrival of spring, the average temperature during COVID-19 lockdown increased by 2.7 °C and 2.1 °C in Hebi and Nanjing, respectively. Based on the thermodynamic theory, we used ISORROPIA-II model to estimate the effects of temperature changes on NH_3 concentrations. The temperature increases favored the gas partitioning of NH_4^+, which increased average NH_3 concentrations only by 0.01 ppb and 0.28 ppb in Hebi and Nanjing, respectively (Fig. S8), indicating that temperature is not the main factor of NH_3 elevation. In addition, ammonia is a common ingredient in household cleaners because it breaks down grease and grime and evaporates quickly (Erdemir and Dincer, 2021). Likely encouraged by the Chinese government's advice to clean frequently touched surfaces and objects regularly to prevent the spread of the coronavirus, the use of home cleaning products has surged dramatically during the lockdown, which would lead to an increase in the emissions of gaseous ammonia. Based on the bottom-up method, the estimated NH_3 emissions increased by 54.3–108.5 Gg during the lockdown period due to the extra use of liquid cleaners in whole China, which only accounts for 6.3%~12.6% of total emissions over the same period (SI Appendix). The emissions from household cleaners could not dominate the NH_3 elevation and due to the lack of direct measurements and detailed activity data, the estimate is still of considerable uncertainty.

Many existing studies have proposed that reduction in SO_2 emissions or NO_x emissions is an important factor in determining the increase in atmospheric NH_3 concentrations on the global and regional scales (Liu et al., 2018; Warner et al., 2017; Yu et al., 2018). The weakened formation of ammonium sulfate/nitrate due to SO_2 and NO_x emission reductions would increase NH_3 concentrations by driving the phase state of NH_3 from particulate to gaseous. By assuming that a 1 mol decrease in simulated NO_3^- would lead to a 1 mol increase in gaseous NH_3 in this region, and 1 mol SO_4^{2-} would lead to 2 mol NH_3 increases (Shen et al., 2018), the simulated increases of surface NH_3 due to the reductions of SO_4^{2-} and NO_3^- are shown in Figs. S9b and S9c. Because the concentrations of particulate sulfate and SO_2 remains relative low during recent years, the limited reduction in SO_2 emissions and the expected subsequent reduction in $(NH_4)_2SO_4$ aerosols have little effect on the increase in free NH_3 (Fig. S9b). The spatial distribution and amount of enhancement NH_3 caused by decreased nitrate (Fig. S9c) are more comparable with the total simulated NH_3 change (Fig. S9a), which infers that the increasing NH_3 was mainly determined by NO_x emission reduction.

The observed molar ratio R (Sect. 2.5) was used to measure the free NH_3 in the atmosphere. In the scenario of $R > 1$, the NH_3 is enough, and almost all particulate NO_3^- exists in the aerosol phase. Due to intensive agricultural activities such as fertilizer application and animal husbandry in the North China Plain, the surrounding area of Hebi (BTH) and Nanjing (YRD) are hotspots of NH_3 loadings. As shown in Fig. 6, in most cases, the R values in the two cities are greater than 1, and during COVID-lock period it was further promoted due to the rising NH_3 concentration.

To study the effect of increasing ammonia (R) on the sink of HNO_3, diagnostic analysis in WRF-Chem was applied to quantify the contributions of atmospheric processes and individual chemical reactions to HNO_3. For all cities, the HNO_3 is dominated by photochemical formation within the region (Fig. 6c). Gas-particle partition, advection transport and dry deposition are the primary "sinks" for HNO_3. By comparing the "reduction" and "no reduction" emission scenarios, the change of HNO_3 photochemical formation in three regions was quite consistent with that of NO_3^-/EC in Fig. 2, which further proves the effects of stronger oxidization during the lockdown. As for the sink, in Beijing, owing to higher photochemical formation rate, the amount of sink during COVID-lockdown has increased. According to the above-identified major formation pathways, rising NH_3 may prompt the partitioning of HNO_3 to the aerosols. However, no change in partitioning/sink ratio was found between the two periods. This is because NH_3 has already been highly in excess (nearly all $R > 1$) before COVID-19 in BTH, so the nitrate formation is less sensitive to NH_3. Due to the insensitivity, nitrate formation does not show a great increase with NH_3 elevation in BTH. Different from BTH, there are some cases $R < 1$ during pre-COVID period in Nanjing and Changsha, indicating that nitrate formation is sometimes NH_3-sensitive. The rising NH_3 favors more gaseous HNO_3 converting to particle phase thus the partitioning/sink ratio is enhanced from 60% to 94% in Nanjing and from 71% to 97% in Changsha. More HNO_3 is converted into particulate form therefore deposition/sink ratio declined from 12% to 5% in Nanjing and from 18% to 2% in Changsha, which means that less HNO_3 is removed from the atmosphere by dry deposition.

The gaseous HNO_3 and particle phase nitrate have different deposition velocities, resulting in different pollution levels. HNO_3 has a fast deposition velocity because of its high solubility, diffusivity and reactivity (Adon et al., 2013), and thus its residence time in the air is quietly short. In NH_3-limited region, the produced HNO_3 can settle down to surface or water and be removed from the atmosphere quickly. However, in NH_3-abundant region, the newly formed gaseous HNO_3 is quickly neutralized by NH_3 and converted to particulate nitrate. Due to large surface resistance (R_s), the deposition velocity of particle phase nitrate is 4–10 times smaller than gaseous HNO_3 under same underlying surface type (McRae, 1982; Hanson and Lindberg, 1991). Thereby, the suspended particulate nitrate can stay in the atmosphere for a relatively long time (days and weeks), continuously accumulating to form haze pollution.

As aforementioned, many factors such as NO_x reduction, meteorological field, increased oxidizing capacity and ammonia, etc., can have

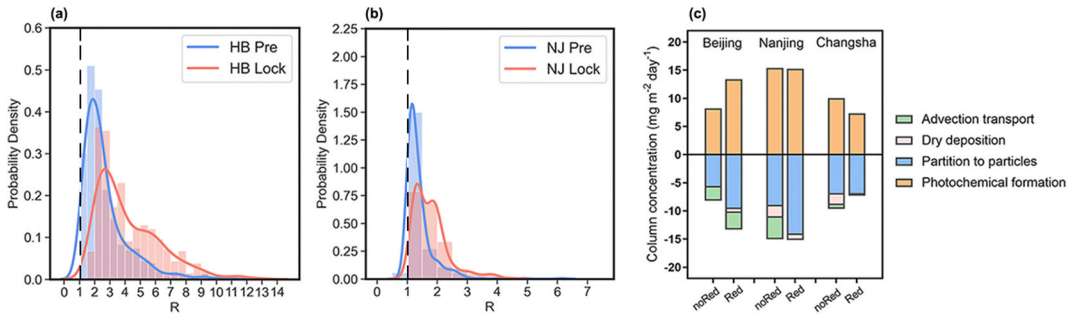

Fig. 6. **(a)** Comparison of probability density distribution of the observed molar ratio R in Hebi station during the COVID-lock (red line) and pre-COVID (blue line) periods. **(b)** Same as (a) but in Nanjing station. The dotted line indicates the position of R = 1. **(c)** Contributions of different atmosphere processes to HNO_3 during the pre-COVID (no Reduction) and COVID-lock (Reduction) periods in Beijing, Nanjing and Changsha three cities. (For interpretation of the references to colour in this figure legend, the reader is referred to the Web version of this article.)

an impact on nitrate concentration. Based on the diagnostic analysis and parallel experiments in WRF-Chem. Fig. 7 gives an estimation about contributions of individual drivers to the nitrate concentrations difference between COVID-lockdown and pre-COVID periods. It is indicated that, for all cities, the nitrate changes were mainly attributed to NO_x emissions reduction. However, with the increase in ambient oxidizing capacity and NH_3, the effect of NO_x reduction on nitrate concentration is partly offset, especially in BTH. Overall, with the joint influence of high concentrations of oxides during COVID-lock period, NO_x can be effectively oxidized into HNO_3, and then neutralized by abundant NH_3 to form particulate nitrate.

4. Conclusions

By integrating ground observations in Beijing, Nanjing and Changsha, the three megacities in eastern China and chemical model simulations, we found a significant reduction in NO_x emissions but less improvement of nitrate pollution during COVID-19. In this work, we investigated the underlying reasons and found the NO_x reduction have side effects on mitigating nitrate pollution. First, dramatic reductions on NO_x emissions in China enhanced O_3 concentration by transforming the sensitivity of O_3 production and reducing NO_x titration. All three cities demonstrated the change of the dominance of the VOCs sensitive regime to the mixed sensitive regime with relatively high O_3 mixing ratios. Therefore, the ground-level observation sites presented a significant increase of O_3 (by ~69%) during COVID-19 outbreak. In addition to observation, the chemical box model and regional transport model were conducted to understand the relationship between NO_x and related oxidation products. The simulations revealed that, due to VOCs limited, the NO_x reduction enhanced ambient OH and NO_3 radicals, and thus facilitated the conversion efficiency of NO_2 to HNO_3. Along with the effective production efficiency caused by higher oxidizing capacity, HNO_3 remained at the previous level although the precursor NO_x has dropped significantly.

Second, NO_x emission reductions reduced the formation of NH_4NO_3 particles and consequently increased the ambient free NH_3 concentrations by 10–40% in northern cities. The sensitivity simulations by fixing the meteorological field of COVID-19 showed that the increased NH_3 favors more HNO_3 partitioning to particle nitrate and lessens HNO_3 dry deposition, especially in NH_3-limited area. Compared with gas phase HNO_3, particle nitrate has a slower deposition velocity and therefore can suspend in the atmosphere for a long time. The higher oxidizing capacity together with increasing ambient NH_3 concentrations resulted in higher production efficiency of NO_x to HNO_3 and gas-particle partition efficiency of HNO_3. Overall, the sharp NO_x reduction and several nitrate pollution during COVID-19 lockdown proved to us that pure NO_x emission reduction is not an effective way to alleviate winter nitrate. Future control strategies for secondary nitrate pollution should not only reduce the emissions of NO_x, but also reduce key oxidants (such as O_3) involved in nitrate production. To minimize the side effects caused by NO_x emission reduction, precise and concurrent NO_x and VOCs emission reductions are needed.

CRediT authorship contribution statement

Chuanhua Ren: Data curation, Visualization, Writing – original draft. **Xin Huang:** Conceptualization, Methodology, Writing – review & editing. **Zilin Wang:** Methodology. **Peng Sun:** Data curation. **Xuguang Chi:** Data curation. **Yue Ma:** Writing – review & editing. **Derong Zhou:** Methodology. **Jiantao Huang:** Data curation. **Yuning Xie:**

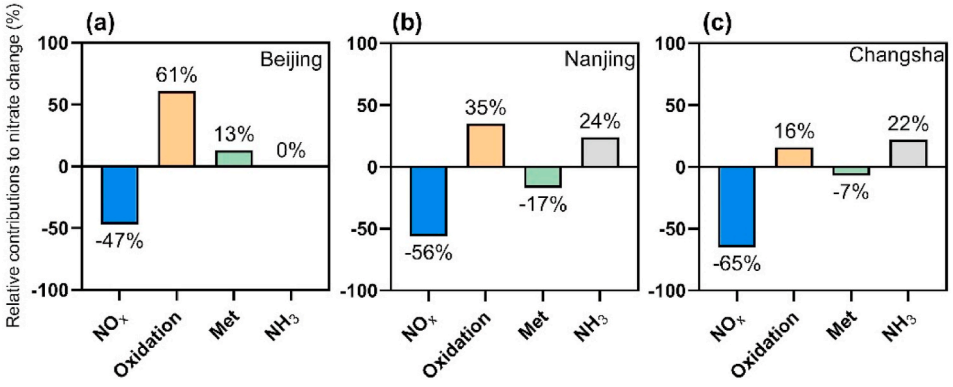

Fig. 7. Contribution of individual drivers to the nitrate concentrations difference between COVID-lockdown and pre-COVID periods in (a) Beijing, (b) Nanjing, and (c) Changsha cities. The drivers include NO_x emissions reduction (blue bar), improving oxidizing capacity (yellow bar), meteorological field (green bar) and increasing NH_3 level (grey bar). (For interpretation of the references to colour in this figure legend, the reader is referred to the Web version of this article.)

Methodology. **Jian Gao:** Methodology. **Aijun Ding:** Supervision, Funding acquisition.

Declaration of competing interest

The authors declare that they have no known competing financial interests or personal relationships that could have appeared to influence the work reported in this paper.

Acknowledgements

This work was supported by the Ministry of Science and Technology of the People's Republic of China (2018YFC0213800), National Natural Science Foundation of China (41875150), the Fundamental Research Funds for the Central Universities (DLTD2107), International cooperation project of Jiangsu Provincial Science and Technology Agency (BZ2017066), Jiangsu Provincial Fund on $PM_{2.5}$ and O_3 pollution mitigation (2019023) and Jiangsu Province Key R&D Program Major Technology Demonstration (BE 2019704). The satellite column concentration of NO_2 used in this work can be acquired from https://acdisc.gesdisc.eosdis.nasa.gov/data/Aura_OMI_Level3/OMNO2d.003/. The global hourly NCDC Integrated Surface Database (ISD) are publicly available from ftp://ftp.ncdc.noaa.gov/pub/data/noaa/. Model outputs are stored in the server of School of Atmospheric Sciences at Nanjing University and are available upon request from the corresponding author.

Appendix A. Supplementary data

Supplementary data to this article can be found online at https://doi.org/10.1016/j.atmosenv.2021.118715.

References

Adon, M., Galy-Lacaux, C., Delon, C., Yoboue, V., Solmon, F., Tchuente, A.T.K., 2013. Dry deposition of nitrogen compounds (NO2, HNO3, NH3), sulfur dioxide and ozone in west and central African ecosystems using the inferential method. Atmos. Chem. Phys. 13, 11351–11374. https://doi.org/10.5194/acp-13-11351-2013.

Brook, R.D., Rajagopalan, S., Pope III, C.A., Brook, J.R., Bhatnagar, A., Diez-Roux, A.V., Holguin, F., Hong, Y., Luepker, R.V., Mittleman, M.A., Peters, A., Siscovick, D., Smith Jr., S.C., Whitsel, L., Kaufman, J.D., Amer Heart Assoc Council, E., Council Kidney Cardiovasc, D., and Council Nutr Phys Activity, M., 2010. Particulate matter air pollution and cardiovascular Disease an update to the scientific statement from the American heart association. Circulation 121, 2331–2378. https://doi.org/10.1161/CIR.0b013e3181dbece1.

Brown, S.S., Stutz, J., 2012. Nighttime radical observations and chemistry. Chem. Soc. Rev. 41, 6405–6447. https://doi.org/10.1039/c2cs35181a.

Calvert, J.G., Stockwell, W.R., 1983. Acid generation in the troposphere by gas-phase chemistry. Environ. Sci. Technol. 17, A428–A443. https://doi.org/10.1021/es00115a002.

Chan, C.K., Yao, X., 2008. Air pollution in mega cities in China. Atmos. Environ. 42, 1–42. https://doi.org/10.1016/j.atmosenv.2007.09.003.

Chang, Y., Huang, R.-J., Ge, X., Huang, X., Hu, J., Duan, Y., Zou, Z., Liu, X., Lehmann, M. F., 2020. Puzzling haze events in China during the coronavirus (COVID-19) shutdown. Geophys. Res. Lett. 47 https://doi.org/10.1029/2020gl088533.

China State Council, 2013. Action Plan on Prevention and Control of Air Pollution. China State Council, Beijing, China http://www.gov.cn/zwgk/2013-09/12/content_2486773.htm. (Accessed 30 September 2018).

Ding, A., Huang, X., Nie, W., Chi, X., Xu, Z., Zheng, L., Xu, Z., Xie, Y., Qi, X., Shen, Y., Sun, P., Wang, J., Wang, L., Sun, J., Yang, X.-Q., Qin, W., Zhang, X., Cheng, W., Liu, W., Pan, L., Fu, C., 2019. Significant reduction of PM2.5 in eastern China due to regional-scale emission control: evidence from SORPES in 2011-2018. Atmos. Chem. Phys. 19, 11791–11801. https://doi.org/10.5194/acp-19-11791-2019.

Ding, A.J., Fu, C.B., Yang, X.Q., Sun, J.N., Zheng, L.F., Xie, Y.N., Herrmann, E., Nie, W., Petaja, T., Kerminen, V.M., Kulmala, M., 2013. Ozone and fine particle in the western Yangtze River Delta: an overview of 1 yr data at the SORPES station. Atmos. Chem. Phys. 13, 5813–5830. https://doi.org/10.5194/acp-13-5813-2013.

Erdemir, D., Dincer, I., 2021. A perspective on the use of ammonia as a clean fuel: challenges and solutions. Int. J. Energy Res. 45, 4827–4834. https://doi.org/10.1002/er.6232.

Filonchyk, M., Peterson, M., 2020. Air quality changes in shanghai, China, and the surrounding urban agglomeration during the COVID-19 lockdown. J. Geovisualization Spatial Anal. 4, 22. https://doi.org/10.1007/s41651-020-00064-5.

Gao, J., Peng, X., Chen, G., Xu, J., Shi, G.-L., Zhang, Y.-C., Feng, Y.-C., 2016. Insights into the chemical characterization and sources of PM2.5 in Beijing at a 1-h time resolution. Sci. Total Environ. 542, 162–171. https://doi.org/10.1016/j.scitotenv.2015.10.082.

Gong, S.L., Barrie, L.A., Blanchet, J.P., 1997. Modeling sea-salt aerosols in the atmosphere .1. Model development. J. Geophys. Res. Atmos. 102, 3805–3818. https://doi.org/10.1029/96jd02953.

Grell, G.A., Peckham, S.E., Schmitz, R., McKeen, S.A., Frost, G., Skamarock, W.C., Eder, B., 2005. Fully coupled "online" chemistry within the WRF model. Atmos. Environ. 39, 6957–6975. https://doi.org/10.1016/j.atmosenv.2005.04.027.

Hanson, P.J., Lindberg, S.E., 1991. Dry deposition of reactive nitrogen-compounds - a review of leaf, canopy and non-foliar measurements. Atmos. Environ. Part a-General Topics 25, 1615–1634. https://doi.org/10.1016/0960-1686(91)90020-8.

Huang, X., Song, Y., Zhao, C., Li, M., Zhu, T., Zhang, Q., Zhang, X., 2014. Pathways of sulfate enhancement by natural and anthropogenic mineral aerosols in China. J. Geophys. Res. Atmos. 119, 14165–14179. https://doi.org/10.1002/2014jd022301.

Huang, X., Ding, A., Gao, J., Zheng, B., Zhou, D., Qi, X., Tang, R., Wang, J., Ren, C., Nie, W., Chi, X., Xu, Z., Chen, L., Li, Y., Che, F., Pang, N., Wang, H., Tong, D., Qin, W., Cheng, W., Liu, W., Fu, Q., Liu, B., Chai, F., Davis, S.J., Zhang, Q., He, K., 2020. Enhanced secondary pollution offset reduction of primary emissions during COVID-19 lockdown in China. Natl. Sci. Rev. https://doi.org/10.1093/nsr/nwaa137.

Huang, X., Tang, G., Zhang, J., Liu, B., Liu, C., Zhang, J., Cong, L., Cheng, M., Yan, G., Gao, W., Wang, Y., Wang, Y., 2021. Characteristics of PM2.5 pollution in Beijing after the improvement of air quality. J. Environ. Sci. 100, 1–10. https://doi.org/10.1016/j.jes.2020.06.004.

Kim, K.-H., Kabir, E., Kabir, S., 2015. A review on the human health impact of airborne particulate matter. Environ. Int. 74, 136–143. https://doi.org/10.1016/j.envint.2014.10.005.

Kong, L., Feng, M., Liu, Y., Zhang, Y., Zhang, C., Li, C., Qu, Y., An, J., Liu, X., Tan, Q., Cheng, N., Deng, Y., Zhai, R., Wang, Z., 2020. Elucidating the pollution characteristics of nitrate, sulfate and ammonium in PM2.5 in Chengdu, southwest China, based on 3-year measurements. Atmos. Chem. Phys. 20, 11181–11199. https://doi.org/10.5194/acp-20-11181-2020.

Leung, D.M., Shi, H., Zhao, B., Wang, J., Ding, E.M., Gu, Y., Zheng, H., Chen, G., Liou, K.-N., Wang, S., Fast, J.D., Zheng, G., Jiang, J., Li, X., Jiang, J.H., 2020. Wintertime particulate matter decrease buffered by unfavorable chemical processes despite emissions reductions in China. Geophys. Res. Lett. 47 https://doi.org/10.1029/2020gl087721.

Li, J., Liao, H., Hu, J., Li, N., 2019. Severe particulate pollution days in China during 2013-2018 and the associated typical weather patterns in Beijing-Tianjin-Hebei and the Yangtze River Delta regions. Environ. Pollut. 248, 74–81. https://doi.org/10.1016/j.envpol.2019.01.124.

Li, M., Zhang, Q., Kurokawa, J.-i., Woo, J.-H., He, K., Lu, Z., Ohara, T., Song, Y., Streets, D.G., Carmichael, G.R., Cheng, Y., Hong, C., Huo, H., Jiang, X., Kang, S., Liu, F., Su, H., Zheng, B., 2017. MIX: a mosaic Asian anthropogenic emission inventory under the international collaboration framework of the MICS-Asia and HTAP. Atmos. Chem. Phys. 17, 935–963. https://doi.org/10.5194/acp-17-935-2017.

Li, M., Wang, T., Xie, M., Li, S., Zhuang, B., Fu, Q., Zhao, M., Wu, H., Liu, J., Saikawa, E., Liao, K., 2020. Drivers for the poor air quality conditions in North China plain during the COVID-19 outbreak. Atmos. Environ. (Oxford, England : 1994). https://doi.org/10.1016/j.atmosenv.2020.118103, 118103-118103.

Liu, M., Huang, X., Song, Y., Xu, T., Wang, S., Wu, Z., Hu, M., Zhang, L., Zhang, Q., Pan, Y., Liu, X., Zhu, T., 2018. Rapid SO_2 emission reductions significantly increase tropospheric ammonia concentrations over the North China Plain. Atmos. Chem. Phys. 18, 17933–17943. https://doi.org/10.5194/acp-18-17933-2018.

Liu, Y., Shen, H., Mu, J., Li, H., Chen, T., Yang, J., Jiang, Y., Zhu, Y., Meng, H., Dong, C., Wang, W., Xue, L., 2021. Formation of peroxyacetyl nitrate (PAN) and its impact on ozone production in the coastal atmosphere of Qingdao, North China. Sci. Total Environ. 778 https://doi.org/10.1016/j.scitotenv.2021.146265.

McRae, G.J., 1982. Dry deposition of nitrogen containing species. Abstr. Pap. Am. Chem. Soc. 183, 71-ENVR.

Pathak, R.K., Wu, W.S., Wang, T., 2009. Summertime PM2.5 ionic species in four major cities of China: nitrate formation in an ammonia-deficient atmosphere. Atmos. Chem. Phys. 9, 1711–1722. https://doi.org/10.5194/acp-9-1711-2009.

Pathak, R.K., Wang, T., Wu, W.S., 2011. Nighttime enhancement of PM2.5 nitrate in ammonia-poor atmospheric conditions in Beijing and Shanghai: plausible contributions of heterogeneous hydrolysis of N2O5 and HNO3 partitioning. Atmos. Environ. 45, 1183–1191. https://doi.org/10.1016/j.atmosenv.2010.09.003.

Peralta, O., Ortinez-Alvarez, A., Torres-Jardon, R., Suarez-Lastra, M., Castro, T., Ruiz-Suarez, L.G., 2021. Ozone over Mexico city during the COVID-19 pandemic. Sci. Total Environ. 761, 143183. https://doi.org/10.1016/j.scitotenv.2020.143183.

Saiz-Lopez, A., Borge, R., Notario, A., Adame, J.A., De la Paz, D., Querol, X., Artinano, B., Gomez-Moreno, F.J., Cuevas, C.A., 2017. Unexpected increase in the oxidation capacity of the urban atmosphere of Madrid, Spain. Sci. Rep. 7 https://doi.org/10.1038/srep45956.

Shen, L., Zhao, T., Wang, H., Liu, J., Bai, Y., Kong, S., Zheng, H., Zhu, Y., Shu, Z., 2021. Importance of meteorology in air pollution events during the city lockdown for COVID-19 in Hubei Province, Central China. Sci. Total Environ. 754 https://doi.org/10.1016/j.scitotenv.2020.142227.

Seinfeld, J.H., Pandis, S.N., 2016. Atmospheric chemistry and physics: From air pollution to climate change, 3rd ed. John Wiley, Hoboken, NJ, pp. 412–414.

Shaw, W.J., Allwine, K.J., Fritz, B.G., Rutz, F.C., Rishel, J.P., Chapman, E.G., 2008. Evaluation of the wind erosion module in DUSTRAN. Atmos. Environ. 42, 1907–1921. https://doi.org/10.1016/j.atmosenv.2007.11.022.

Shen, Y., Virkkula, A., Ding, A., Wang, J., Chi, X., Nie, W., Qi, X., Huang, X., Liu, Q., Zheng, L., Xu, Z., Petaja, T., Aalto, P.P., Fu, C., Kulmala, M., 2018. Aerosol optical properties at SORPES in Nanjing, east China. Atmos. Chem. Phys. 18, 5265–5292. https://doi.org/10.5194/acp-18-5265-2018.

Sun, P., Nie, W., Chi, X., Xie, Y., Huang, X., Xu, Z., Qi, X., Xu, Z., Wang, L., Wang, T., Zhang, Q., Ding, A., 2018. Two years of online measurement of fine particulate nitrate in the western Yangtze River Delta: influences of thermodynamics and N2O5 hydrolysis. Atmos. Chem. Phys. 18, 17177–17190. https://doi.org/10.5194/acp-18-17177-2018.

Wang, Z, Huang, X, Ding, A, 2018. Dome effect of black carbon and its key influencing factors: a one-dimensional modelling study. Atmos. Chem. Phys. 2821–2834.

Wang, T., Huang, X., Wang, Z., Liu, Y., Zhou, D., Ding, K., Wang, H., Qi, X., Ding, A., 2020. Secondary aerosol formation and its linkage with synoptic conditions during winter haze pollution over eastern China. Sci. Total Environ. 730 https://doi.org/10.1016/j.scitotenv.2020.138888.

Wang, Y., Li, W., Gao, W., Liu, Z., Tian, S., Shen, R., Ji, D., Wang, S., Wang, L., Tang, G., Song, T., Cheng, M., Wang, G., Gong, Z., Hao, J., Zhang, Y., 2019. Trends in particulate matter and its chemical compositions in China from 2013-2017. Sci. China Earth Sci. 62, 1857–1871. https://doi.org/10.1007/s11430-018-9373-1.

Wang, T., Xue, L., Brimblecombe, P., Lam, Y.F., Li, L., Zhang, L., 2017. Ozone pollution in China: A review of concentrations, meteorological influences, chemical precursors, and effects. Sci. Total Environ. 575, 1582–1596. https://doi.org/10.1016/j.scitotenv.2016.10.081.

Warner, J.X., Dickerson, R.R., Wei, Z., Strow, L.L., Wang, Y., Liang, Q., 2017. Increased atmospheric ammonia over the world's major agricultural areas detected from space. Geophys. Res. Lett. 44, 2875–2884. https://doi.org/10.1002/2016GL072305.

Wen, L., Xue, L., Wang, X., Xu, C., Chen, T., Yang, L., Wang, T., Zhang, Q., Wang, W., 2018. Summertime fine particulate nitrate pollution in the North China Plain: increasing trends, formation mechanisms and implications for control policy. Atmos. Chem. Phys. 18, 11261–11275. https://doi.org/10.5194/acp-18-11261-2018.

World Health Organization Occupational and Environmental Health Team, 2006. WHO Air Quality Guidelines for Particulate Matter, Ozone, Nitrogen Dioxide and Sulfur Dioxide: Global Update 2005: Summary of Risk Assessment. World Health Organization.

Xie, Y., Ding, A., Nie, W., Mao, H., Qi, X., Huang, X., Xu, Z., Kerminen, V.-M., Petaja, T., Chi, X., Virkkula, A., Boy, M., Xue, L., Guo, J., Sun, J., Yang, X., Kulmala, M., Fu, C., 2015. Enhanced sulfate formation by nitrogen dioxide: implications from in situ observations at the SORPES station. J. Geophys. Res. Atmos. 120, 12679–12694. https://doi.org/10.1002/2015jd023607.

Xinhua News, 2020. 30 Provinces Activated First-Level Public Health Emergency Response accessed 2020-01-25. http://www.xinhuanet.com/politics/2020-01/25/c_1125502232.htm.

Xu, P., Chen, Y., Ye, X., 2013. Haze, air pollution, and health in China. Lancet 382, 2067. https://doi.org/10.1016/s0140-6736(13)62693-8.

Xu, Q., Wang, S., Jiang, J., Bhattarai, N., Li, X., Chang, X., Qiu, X., Zheng, M., Hua, Y., Hao, J., 2019a. Nitrate dominates the chemical composition of PM2.5 during haze event in Beijing, China. Sci. Total Environ. 689, 1293–1303. https://doi.org/10.1016/j.scitotenv.2019.06.294.

Xu, W., Zhang, G., Wang, Y., Tong, S., Zhang, W., Ma, Z., Lin, W., Kuang, Y., Yin, L., Xu, X., 2021. Aerosol promotes peroxyacetyl nitrate formation during winter in the North China plain. Environ. Sci. Technol. 55, 3568–3581. https://doi.org/10.1021/acs.est.0c08157.

Xu, Z., Liu, M., Zhang, M., Song, Y., Wang, S., Zhang, L., Xu, T., Wang, T., Yan, C., Zhou, T., Sun, Y., Pan, Y., Hu, M., Zheng, M., Zhu, T., 2019b. High efficiency of livestock ammonia emission controls in alleviating particulate nitrate during a severe winter haze episode in northern China. Atmos. Chem. Phys. 19, 5605–5613. https://doi.org/10.5194/acp-19-5605-2019.

Yang, F., Tan, J., Zhao, Q., Du, Z., He, K., Ma, Y., Duan, F., Chen, G., Zhao, Q., 2011. Characteristics of PM2.5 speciation in representative megacities and across China. Atmos. Chem. Phys. 11, 5207–5219. https://doi.org/10.5194/acp-11-5207-2011.

Yang, G., Liu, Y., Li, X., 2020. Spatiotemporal distribution of ground-level ozone in China at a city level. Sci. Rep. 10, 7229. https://doi.org/10.1038/s41598-020-64111-3.

Yu, F., Nair, A.A., Luo, G., 2018. Long-term trend of gaseous ammonia over the United States: modeling and comparison with observations. J. Geophys. Res. Atmos. 123, 8315–8325. https://doi.org/10.1029/2018JD028412.

Yu, Y., Ding, F., Mu, Y., Xie, M., Wang, Q.g., 2020. High time-resolved PM2.5 composition and sources at an urban site in Yangtze River Delta, China after the implementation of the APPCAP. Chemosphere 261. https://doi.org/10.1016/j.chemosphere.2020.127746.

Zaveri, R.A., Peters, L.K., 1999. A new lumped structure photochemical mechanism for large-scale applications. J. Geophys. Res. Atmos. 104, 30387–30415. https://doi.org/10.1029/1999jd900876.

Zhang, Q., Zheng, Y., Tong, D., Shao, M., Wang, S., Zhang, Y., Xu, X., Wang, J., He, H., Liu, W., Ding, Y., Lei, Y., Li, J., Wang, Z., Zhang, X., Wang, Y., Cheng, J., Liu, Y., Shi, Q., Yan, L., Geng, G., Hong, C., Li, M., Liu, F., Zheng, B., Cao, J., Ding, A., Gao, J., Fu, Q., Huo, J., Liu, B., Liu, Z., Yang, F., He, K., Hao, J., 2019. Drivers of improved PM2.5 air quality in China from 2013 to 2017. Proc. Natl. Acad. Sci. U.S.A. 116, 24463–24469. https://doi.org/10.1073/pnas.1907956116.

Zheng, B., Zhang, Q., Geng, G., Chen, C., Shi, Q., Cui, M., Lei, Y., He, K., 2021. Changes in China's anthropogenic emissions and air quality during the COVID-19 pandemic in 2020. Earth Syst. Sci. Data 13, 2895–2907. https://doi.org/10.5194/essd-13-2895-2021.

Further reading

Lin, Yuh-Lang, RichardFarley, D., HaroldOrville, D., 1983. Bulk Parameterization of the Snow Field in a Cloud Model. J. Appl. Meteorol. Climatol. 22 (6), 1065–1092.